Published in final edited form as:
Biochemistry. 2012 March 27; 51(12): 2579–2587. doi:10.1021/bi300057q.

Structure of the *S. aureus* PI-specific phospholipase C reveals modulation of active site access by a titratable π-cation latched loop†

Rebecca Goldstein‡, **Jiongjia Cheng**‡, **Boguslaw Stec**§, and **Mary F. Roberts**‡,*
‡Department of Chemistry, Boston College, Chestnut Hill, Massachusetts 02467
§Sanford-Burnham Medical Research Institute, La Jolla, California

Abstract

Staphylococcus aureus secretes a phosphatidylinositol-specific phospholipase C (PIPLC) as a virulence factor that is unusual in exhibiting higher activity at acidic pH values than other enzymes in this class. We have determined the crystal structure of this enzyme at pH 4.6 and pH 7.5. Under slightly basic conditions, the *S. aureus* PI-PLC structure closely follows the conformation of other bacterial PI-PLCs. However, when crystallized under acidic conditions, a large section of mobile loop at the αβ-barrel rim in the vicinity of the active site shows ~10 Å shift. This loop displacement at acidic pH is the result of a titratable intramolecular π-cation interaction between His258 and Phe249. This was verified by a structure of the mutant protein H258Y crystallized at pH 4.6, which does not exhibit the large loop shift. The intramolecular π-cation interaction for *S. aureus* PI-PLC provides an explanation for the activity of the enzyme at acid pH and also suggests how phosphatidylcholine, as a competitor for Phe249, may kinetically activate this enzyme.

Phosphatidylinositol-specific phospholipase C (PI-PLC) is a virulence factor produced and secreted by many Gram positive bacteria (1). When secreted by extracellular pathogens (e.g., *Bacillus* and *Staphylococcus* strains (2–5) this enzyme catalyzes the cleavage of glycan-phosphatidylinositol (GPI) anchored proteins. PI-PLC removal of the protective GPI-anchored proteins on the exterior surface of mammalian cells allows cellular damage to occur, and the diacylglycerol, translocating across the bilayer (6), can interfere with cellular signaling processes (7). Phosphatidylinositol molecules are also good substrates for this enzyme and provide an easier system to explore mechanistic details of these enzymes (1). PI-PLC cleaves its substrate via an intramolecular phosphotransferase reaction on the PI moiety to form a cyclic inositol phosphate molecule and diacylglycerol (8). Subsequent hydrolysis of the cyclic phosphodiester produces inositol 1-phosphate if PI is the substrate (9, 10). The PI-PLC from *S. aureus* is unusual in exhibiting significant activity towards PI at acidic pH (4) – a property that may contribute to the virulence of the organism, which is often in an acidic milieu (11).

Crystal structures of the PI-PLC enzymes from *Bacillus* species (12, 13) and *Listeria monocytogenes* (14), an intracellular pathogen, show very similar distorted TIM barrels with an active site close to the barrel rim. Each has a short helix at the rim that contains at least one lysine, important for binding to negatively charged interfaces, and a tryptophan that, in the case of the *Bacillus* PI-PLC, has been proposed to insert into target membranes (15–17).

†This research was supported by NIH Grant GM60418 (M.F.R.).

*To whom correspondence should be addressed. Phone: (617) 552-3616. Fax: (617) 552-2705. mary.roberts@bc.edu.

Another key structural feature is a rim loop near the active site that contains one large hydrophobic residue (either a tryptophan or phenylalanine) amid many small flexible residues. This surface-exposed hydrophobic residue is also thought to aid in anchoring the protein to membranes (15, 16).

Several of the bacterial PI-PLC enzymes exhibit kinetic activation by non-substrate phospholipids. Specifically, inclusion of PC in vesicles containing PI lead to large increases in the specific activity of these secreted PI-PLC enzymes (9, 18, 19). The detailed mechanism for PC activation is not the same for the different enzymes. *B. thuringiensis* PI-PLC has a discrete site for PC binding (20), while the *L. monocytogenes* PI-PLC requires PC to dilute cationic enzyme/anionic lipid aggregates that trap the enzyme in a nonproductive state (19). The PI-PLC from *S. aureus* can also exhibit a significant increase in specific activity towards PI in vesicles containing PC (*vide infra*).

We have solved the structure of *S. aureus* PI-PLC strain FPR3757 at two different pH values: (i) pH 4.6, where the enzyme shows low activity (but significantly higher than other bacterial PI-PLC enzymes), and (ii) pH 7.5, where it is very active towards PI/PC (but not pure PI) vesicles. A large conformational change in the rim mobile loop between the acidic and basic pH structures depends on a titratable π-histidine cation interaction. π-Cation interactions are well known in proteins, however these interactions commonly exist in protein-protein interfaces, enzyme-drug interactions, helix stabilization and protein-DNA interactions (21–23). π-Cation complexes with protonated histidine as the cation are also known (24). Most of these interactions result in subtle structural changes; typically they mediate ligand binding or helix stabilization (25, 26). However, a recent structure of the transferrin receptor showed a large change in structure in the dimer interface region upon transferrin binding whereby a protonated surface histidine flipped into the protein to engage in π-stacking with a phenylalanine and tyrosine (27).

Observation of the titratable intramolecular π-cation interaction in *S. aureus* PI-PLC suggests higher activity at acidic pH is connected with easier release of water-soluble product inositol 1,2-(cyclic)phosphate (cIP). This structural feature also provides an explanation for how PC may activate this bacterial PI-PLC. The presence of that zwitterionic phospholipid in a substrate-containing interface provides cationic choline moieties that can compete with cationic His258 for interactions with the π system of Phe249 allowing the latter to partition into membranes. The higher activity once PC is added indicates that this membrane conformation must differ from the one where only PI is present.

Experimental Procedures

Expression and Purification

The genomic DNA of *S. aureus* (strain FPR3757) was purchased from ATCC and the gene coding for PI-PLC was amplified by PCR, cleaved by the restriction enzymes *EcoR1* and *Xhol* (New England BioLabs, Inc.), and inserted in to the vector (pET21a) with a C-terminal hexa-histidine tag. The sequence of this gene, confirmed by Genewiz, was equivalent to that reported previously (4). For producing the H258Y mutant protein, QuickChange methodology with the site-directed mutagenesis kit from Stratagene and the complimentary primer purchased from Operon were used. The sequence of the mutated gene was confirmed by Genewiz. The plasmids containing the two PI-PLC genes were transformed into *E. coli* BL21-Codonplus (DE3)-RIL cells. Overexpression of the proteins followed protocols used for the *B. thuringiensis* PI-PLC (15). The *S. aureus* PI-PLC proteins were purified in two steps: (i) lysed cell pellets were mixed with an Ni-NTA resin (Qiagen) and an imidazole gradient used to elute the PI-PLC; (ii) after overnight dialysis in 20 mM Tris, pH 8.3, the

protein solution was further purified by elution from a Q-Sepharose fast-flow anion-exchange resin. The concentration of the PI-PLC enzymes, greater than 95% pure as monitored by SDS-PAGE, was measured by the absorption at 280 nm using an extinction coefficient calculated by the web-based ProtParam software. The yield of purified protein was 60 mg/L cell culture.

Crystallography

Purified PI-PLC was concentrated to 20 mg/mL before being combined with *myo*-inositol. The protein solution was then diluted to 10 mg/mL using deionized water and incubated on ice for a minimum of two hours before setting up crystallization trays. For determination of initial conditions, Qiagen JCSG core 1 and 2 screens were used. All PI-PLC samples were crystallized at 20°C by vapor diffusion, using hanging drops of 3 μL, at a final protein concentration of 10 mg/mL. Suitable crystals were mounted in nylon loops and frozen in liquid nitrogen.

For the basic pH structure, PI-PLC was crystallized in 10% isopropanol, 100 mM HEPES, pH 7.5, with 20% PEG 4000. Single crystals developed after approximately one week and grew to a final size of approximately 0.2 mm in length. For the acidic pH structure, the protein crystallized in 150 mM ammonium acetate, 100 mM sodium acetate, pH 4.6, with 10 mM magnesium nitrate, and 20% PEG 4000. Prior to crystallization, the protein was incubated with 100 mM myo-inositol and 5 mM diC_6PC (Avanti Polar Lipids). Suitable crystals presented as large plates (0.5–0.7 mm in length), which appeared in the drop after approximately three months. The H258Y structure was crystallized in 150 mM ammonium acetate, 100 mM sodium acetate pH 4.6, 100 mM magnesium nitrate, and 26% PEG 4000. Prior to crystallization the protein was incubated with 100 mM myo-inositol. Single crystals appeared after two days and grew to a size of 0.4 mm in length.

Data were collected at 100 K using an in-house Rigaku MicroMax-07 HF high intensity microfocus rotating Cu anode X-ray generator, coupled with Osmic VariMax Optics and a R-Axis IV++ image plate area detector. Data were indexed and reduced using HKL2000 (28). The acidic pH structure was solved by molecular replacement in CCP4 (29), using PHASER (30) in CCP4, with the *B. cereus* structure 1PTG (12) as a model. The basic and mutant structures were solved similarly using the acidic structure as a model. All models were initially refined using CNS (31), then reanalyzed and refined with Refmac (29), with manual model building in COOT (32). Maps generated in PHENIX (33), and manual model building in COOT (32). Ligands and ligand restraints were generated using Prodrg2 (34). Structural comparisons were made using SSM superposition (35) in COOT and alignment in Pymol (36). Adit (37) was used for structure validation.

PI-PLC kinetics

The specific activity of the recombinant *S. aureus* PI-PLC enzymes was measured towards small unilamellar vesicles (SUVs) of bovine brain PI (4 mM) and PI/PC (4 mM:1 mM) using ^{31}P NMR spectroscopy (Varian INOVA 600) to analyze product generation at fixed time points as described previously for the *B. thuringiensis* PI-PLC (16). The particular PC species used was 1-palmitoyl-2-oleoyl-PC (Avanti Polar Lipids). SUVs were prepared by sonicating the dispersed phospholipid solution on ice for 20 s, then off for 20 s, for a total time of 20 min. Vesicle sizes of PI containing SUVs prepared this way were quite similar for up to 50 % PC (38) as estimated by light scattering. For pure PI SUVs in MES, H 6.5, the average radius was 133 Å with a 20.4% polydispersity; for PI/PC (1:1) SUVs, the average radius was 127 Å with 42.6% polydispersity. The enzyme (4 μg/mL for pure PI SUVs and 1 μg/mL for the PI/PC mixed SUVs) was incubated with the vesicles for fixed times (selected to ensure <20% PI cleavage) at 28 °C; the reaction was quenched with acetic acid (dropping

the pH below 4) followed by the addition of the Triton X-100 to solubilize the remaining lipids in mixed micelles. The relative integrated intensity of the cIP resonance versus the total phospholipid concentration (initial [PI] or [PI]+[PC]) was used to calculate PI-PLC specific activity. The buffer was 50 mM MES/HEPES with the pH adjusted to pH 5.5, 6.5, or 7.5; all buffers included 1 mM EDTA and 0.1 mg/mL BSA (used to stabilize the protein at the very low concentrations used in these assays).

A qualitative turbidity assay was used to compare the ability of short-chain phospholipids with different head groups to alter PI (4 mM) cleavage when it was dispersed in Triton X-100 (8 mM) micelles in MES buffer at pH 6.5. The lipids added included 16 mM of diC_7PC, diC_8PE, diC_8PG or diC_8PS.

Results and Discussion

Structure of S. aureus PI-PLC

All three forms of *S. aureus* PI-PLC (wild type, acidic and basic conditions, and H258Y) crystallized as monomers in the $P2_12_12_1$ space group. Data for the acidic structure were collected at a resolution of 2.3 Å and refined to a final R value of 15.6% (R_{free}=21.3%); the unit cell, with dimensions a=104.16, b=43.61 and c=62.22 Å, contained myo-inositol in the active site, and one chloride ion. Electron density contoured to 1σ for the rim loop with the model superimposed is shown in Figure 1. Although the acidic form of PI-PLC was co-crystallized with 5 mM dihexanoyl-PC, no discrete density for phospholipid was observed in the crystal structure. However, there was a significant improvement in crystal stability when that short-chain phospholipid was present in the crystallization medium. Data for the basic pH structure were collected at a resolution of 2.3 Å and refined to a final R value of 18.2% (R_{free}=25.6%); this unit cell, with dimensions, a=85.47, b=57.95 and c=61.74 Å, contained one sulfate ion. The H258Y mutant structure, with data collected at a resolution of 1.9 Å and refined to a final R value of 18.7% (R_{free}= 23.7%), was found to contain myo-inositol and two acetate anions. Interestingly, H258Y, though crystallized under acidic conditions, had a unit cell almost identical to that of the basic structure of wild type recombinant PI-PLC. Table 1 summarizes crystallographic data and refinement statistics for the three different crystals.

Similar to the other bacterial PI-PLC crystal structures (12–14) in the database, the enzyme from *S. aureus* folds into an imperfect $(\beta\alpha)_8$-barrel. Notation of the helices, following the other bacterial PI-PLC structures, is shown in Figure 1B. The mature *S. aureus* PI-PLC begins with Ser1, as noted previously (4). The overall structure of the *S. aureus* PI-PLC obtained at pH 7.5 is most similar to *B. thuringiensis* (3EA2) and *B. cereus* PI-PLC (1PTG) structures (12, 13). Figure 1C compares the basic structure of the *S. aureus* protein to the *B. cereus* PI-PLC. Density for Ser1 was observed in the acidic structure, while density began at Asp2 in both the basic and H258Y structures. In two of these *S. aureus* PI-PLC structures, a portion of the uncleaved C-terminal His_6 tag was visible extending from the C-terminus of the protein. In the acidic structure, density extended to Leu303, in the basic pH structure, density extended to His305, and in H258Y it extended to His308. Active site residues (and electrostatic maps of the active site) in all three *S. aureus* PI-PLC structures are well conserved, with all catalytic residues remaining relatively unchanged in both position and rotamer. Additionally, myo-inositol binding remains the same in both the acidic and H258Y mutant *S. aureus* PI-PLC structures.

Two key structural features of the Bacillus enzymes are short helix B and a mobile rim loop, both of which have been implicated in membrane binding (15–17, 20). Helix B in *S. aureus* PI-PLC (^{41}V-K-S-V-W-A-K) is one residue longer than in the *B. cereus* structures. It also has two lysine residues making a more positively charged feature. This, in conjunction with

the other rim positively charged residues (Lys209, Lys113 Lys114, Lys121, and Arg69), forms an extended region of positive charge along the barrel rim and would suggest that membrane binding (at least to substrate membranes with moderate negative charge) is largely driven by electrostatics (Figure 3). Additionally, a bound anion is seen in each structure in a conserved position in a cationic pocket on the rim, composed of the side chains of His86, Lys42, and the backbone amides of Lys38 and Asp39. The identity of the bound ligand changes with each structure: the pH 7.5 structure contains a sulfate, the pH 4.6 structure contains a chloride, and the H258Y structure contains an acetate anion. However, in all *S. aureus* PI-PLC crystal structures there is an anion present in this highly electropositive pocket. The position of this bound anion near at the rim surface is where one might expect the head group of an anionic phospholipid to bind.

The mobile rim loop contributes a key hydrophobic residue, Trp242 in *Bacillus* PI-PLC and Phe237 in the *L. monocytogenes* structure) to membrane binding (12–14). The analogous residue in the basic *S. aureus* PI-PLC structure, Phe249, is pointed towards the membrane interface, slightly above the lip of the (βα)8-barrel (Figure 2 suggests the membrane-binding orientation by a gray line). However, in the *B. cereus* structure, that side chain is pointed down, along the axis of the (βα)8-barrel between helixes G and H, and away from the membrane interface (12). Similarly, in *L. monoccytogenes* PI-PLC the equivalent residue (Phe237) is again pointed away from the membrane interface, though in that structure it flanks helix G on the opposite side. This stresses the flexibility of the rim loop and the Trp/Phe side chain position in the different bacterial PI-PLC proteins.

It is this loop of the *S. aureus* protein that undergoes the largest change in structure with pH (Figures 2 and 4). In the acidic form of PI-PLC, the π system of Phe249 forms a π-cation complex with protonated His258. This draws Phe249 down between helixes F and G and leads to a condensed conformation of the rim loop – the π-cation complex acts as a latch to restrain the loop close to the protein surface. This position for the Phe side chain is similar to that of Phe237 in *L. monocytogenes* PI-PLC, However, *L. monocytogenes* PI-PLC has an alanine in the position corresponding to His258, thus no π-cation complex can be formed. Although Phe237 is pointed down between two helixes, it is shifted upward 3.1 Å from its *S. aureus* PI-PLC equivalent. Without the π-cation complex, the loop is held in an extended conformation in the *L. monocytogenes* PI-PLC. Additionally in *S. aureus* PI-PLC, the loop is most stable in the acidic form, with excellent coverage of electron density (see Figure 1) and relatively low B-factors. In the basic form, the rim loop is significantly more mobile, with higher B-factors and less complete electron density. This trend is mirrored in the H258Y mutant, where the loop is again in its extended and significantly more mobile position. Crystal packing has no effect on the mobile loop. In the basic form of the structure, the closest crystallographic neighbors are about 6-8 Å away. The H258Y form of the structure shows one crystallographic neighbor 4.5 Å from Asn250, though this neighbor does make contact within the structure. Rather, it hydrogen bonds with Asn254, and does not affect the loop. Finally, in the acidic structure, one hydrogen bond is made between the backbone carbonyl of Ala248 and the side chain amide of neighboring Asn10. However, crystal packing would not have sterically hindered this conformation if the loop had adopted the extended position in this structure, Therefore, the difference in loop conformations is not an artifact of crystal packing but a conformational change in response to the protonation state of the protein.

pH Dependent π-Cation

Aside from the mobile loop and a few aromatic residues with different rotamers, (Tyr211, Tyr212, and Tyr255 move to accommodate Phe249, and Trp45 in helix B moves to accommodate the mobile loop in the acidic pH structure) the enzyme side chains are largely unchanged between the acidic and basic pH structures. The rim loop undergoing the pH-

dependent movement consists of eleven residues (^{241}S-V-A-S-G-G-S-A-F-N-S). It shows a maximum backbone displacement of 9.4 Å between the acidic and basic forms of *S. aureus* PI-PLC, as measured at the α-carbon of Ser247. At pH 4.6, the cationic nitrogen on His258 is positioned 3.5 Å from the π system of Phe249, which itself is 3.5 Å from that of Tyr212 in a face-edge interaction. The π-cation interaction holds Phe249, and thus the rest of the mobile loop in a position where Phe249, the lone hydrophobic residue in the mobile rim loop, is unable to partition into membranes (Figure 4A). At pH 7.5, His258 will be deprotonated. With the cation no longer present, the rim loop reverts to the more extended loop position, approximately 10 Å away (Figure 4B), where His258 is 11.7 Å away from the π system of Phe249. Similarly, His258 is 4.6 Å from Tyr212.

Interestingly, the large pH-dependent structural change we see is reminiscent of what is seen in the homodimeric transferrin receptor (TFR) when its ligand, the human transferring molecule (hTF) binds the apo homodimer at biological pH. Binding of hFT to TRF at pH 7.4 causes two dimer interface tryptophan residues per monomer to switch from π-π stacking interactions to formation of π-cation interactions. The switch in these interactions causes rotation of the dimer interface, which primes the homodimer for chain reaction at the interface when endosomal pH is encountered, resulting in the rapid release of the iron held by the hFT/TFR complex (27). Though not specifically an intraprotein movement, this dimer rotation further emphasizes the importance of these increasingly encountered π-cation interactions.

H258Y – abolishing the intramolecular π-cation interaction

To confirm that the mobile loop conformational switch is dependent on a π-cation interaction between Phe249 and His258, the mutant protein H258Y was prepared and crystallized. The H258Y mutation eliminates any possibility of a titratable π-cation interaction in *S. aureus* PI-PLC. The crystal structure obtained a pH 4.6 (Figure 4C) shows the mobile loop in an extended position similar to that of the native PI-PLC structure under basic conditions. Additional crystal structures of native *S. aureus* PI-PLC at both pH 4.6 and 7.5 with or without myo-inositol and other ligands (unpublished data) show a strong trend. This enzyme will crystallize in one of two unit cells in a pH dependent manner in a very consistent basis. At pH 4.6, *S. aureus* PI-PLC crystallizes with an average unit cell of a=104.01 Å, b=43.57Å, and c=62.17Å; at pH 7.5 it crystallizes with an average unit cell of a=85.68Å, b=58.22 Å, and c=61.65 Å. This trend with pH is only broken by the H258Y structure. Although crystallized at pH 4.6, it has a unit cell consistent with the basic form of native enzyme. Thus, the determining factor between the two unit cells appears to be the position of the mobile loop, rather than pH alone. The H258Y mutation prevents the π-cation interaction and the mutant crystallizes with the mobile rim loop in an extended conformation. The H258Y structure confirms that the mobile loop conformational change is the result of the protonation state of His258 and the resulting π-cation interaction.

Activity of S. aureus PI-PLC

Given the two discrete conformations adopted by *S. aureus* PI-PLC, two questions need to be addressed. (i) How are the two conformations related to enzymatic activity? (ii) Does this pH-dependent change have a physiological role in *S. aureus* infectivity? To explore the first, we have measured PI-PLC activity toward small unilamellar vesicles composed of either pure PI or PI/PC (4:1) at pH 5.5, 6.5, and 7.5. The enzyme binds tightly to vesicles with phosphatidylglycerol replacing PI and small amounts of the non-substrate PC (J. Cheng, unpublished results). The PI-PLC enzyme mechanism involves two histidine residues acting as a general base and general acid (1, 10). If the π-cation interaction in *S. aureus* PI-PLC modulates activity, it may be difficult to sense since it also involves a histidine residue.

However, we can examine activity of H258Y as a control that cannot form the intramolecular π-cation interaction.

As shown in Figure 5, a comparison of activities towards PI vesicles at pH 5.5, 6.5, and 7.5 show that the recombinant enzyme has higher activity at pH 5.5, where the π-cation interaction and inward-folded orientation of the rim loop occur, than H258Y. Specific activities are similar and lower for both enzymes as the pH increases (and presumably the π-His-cation interaction is broken). When 20 mol% PC is present in the vesicles, the activities are low at pH 5.5 but increase as the pH is raised. Wild type enzyme shows higher activity at pH 6.5 than H258Y. If the only difference is the formation of the π-cation interaction, it appears that the presence of PC may alter the pKa values for the catalytic His residues and possibly the His in the π-cation interaction as well. Regardless of the presence of PC, the inward-folded rim loop position appears to be associated with higher enzymatic activity at acidic pH.

Previous work has shown that this PI-PLC, with an acidic pH optimum, is extremely sensitive to added salt (4). Such behavior is consistent with electrostatic forces dominating partitioning of the protein onto membranes and binding of an individual substrate in the active site. Our structural analysis emphasizes the cationic character of the rim and active site that would be responsible for such behavior (Figure 3). However, we can obtain insight into the activity at acidic pH by looking at space-filling models of the *S. aureus* PI-PLC at the two pH values (Figure 6). Access of substrate to the active site from the membrane face is apparent in both structures. However, a side view, that should detect an exit path for the water-soluble product cIP with the protein still attached to the membrane, shows access to the active site *only* in the acidic pH structure. In the basic structure, the loop is extended but active site access via other than the membrane interface is restricted. The two conformations of Trp45 appear to be linked to restricting access to the active site (Figure 7). This suggests the one function of the π-cation latch is to ensure water-soluble product can diffuse from the active site and into bulk solution. It allows for at least some degree of processive catalysis for this enzyme bound to membranes under acidic conditions.

The shift in the PI-PLC activity profile with 20 mol% PC present in the bilayer suggests that the phospholipid choline moiety, among other effects, can compete with His258 for interaction with Phe249. At pH 5.5 both wild type and H258Y exhibit low specific activities. We now have an extended loop, which may allow membrane partitioning of the protein, but not easy release of the water-soluble product. Increasing the pH enhances activities above what is seen in the absence of PC – a result that suggests other more subtle conformational changes in the protein occur with PC added. The pKa values for the general base and general acid histidines may be shifted when PC is present. Whatever the discrete changes, the structure suggests that PC could compete for Phe249 and the extended loop structure can lead to more efficient PI cleavage and product release.

Consistent with the idea that the choline cation competes with His258 we have examined the effect of different short-chain phospholipids on cleavage of PI dispersed in Triton X-100 micelles. The use of the Triton micelle matrix and micelle forming additives should avoid changes in bilayer behavior that may occur with the different long-chain phospholipids (PE in particular). In this qualitative turbidity assay it is clear that both diC_7PC and diC_8PE activate the enzyme above what is observed with the PI dispersed in TX-100, while diC_8PG and diC_8PS are inhibitory (roughly 10-fold less active than with the short-chain PC added), presumably by binding to the active site. The amino group of PE, like the trimethylammonium group of PC, could interact with Phe249 and similarly alter pKa values or lead to a more productive conformation involving that rim loop.

Connecting the π-cation latched loop with S. aureus infection?

S. aureus is known to cause a broad range of diseases in humans, and is commonly found in skin infections and abscesses which can lead to toxemia and lethal bacteremia (7, 39). Secreted *S. aureus* PI-PLC may aid in colonization and replication of the microorganism by generating diacylglycerol from GPI-anchored proteins. It is one of the exoproteins shown to be upregulated upon infection in community-associated methicillin-resistant *Staphylococcus aureus* (40). This may be part of the response of *S. aureus* in coopting the immune response of host cells. The pH of an *S. aureus* abscess decreases to 6.6 – the pH optimum of *S. aureus* PI-PLC (4, 11). Our kinetic studies also show that in bilayers with PC as well as PI, the pH optimum for this enzyme is around this value.

Abbreviations

cIP	inositol 1,2-(cyclic)phosphate
diC$_6$PC	1,2-dihexanoyl-sn-glycero-3-phosphocholine
diC$_7$PC	diheptanoyl-PC
diC$_8$PE	1,2-dioctanoyl-sn-glycero-3-phosphoethanolamine
diC$_8$PG	1,2-dioctanoyl-sn-glycero-3-phosphoglycerol
diC8PS	1,2-dioctanoyl-sn-glycero-3-phosphoserine
GPI	glycan-phosphatidylinositol
PC	phosphatidylcholine
PEG	poly(ethylene glycol)
PI	phosphatidylinositol
PI-PLC	phosphatidylinositol-specific phospholipase C

References

1. Griffith OH, Ryan M. Bacterial phosphatidylinositol-specific phospholipase C: structure, function, and interaction with lipids. Biochim. Biophys. Acta. 1999; 1441:237–254. [PubMed: 10570252]
2. Rhee SG, Suh PG, Ryu S, Lee SY. Studies of inositol phospholipids-specific phospholipase-C. Science. 1989; 244:546–550. [PubMed: 2541501]
3. Kyei-Poku G, Gauthier D, Pang A, van Frankenhuyzen K. Detection of *Bacillus cereus* virulence factors in commercial products of *Bacillus thuringiensis* and expression of diarrheal enterotoxins in a target insect. Can. J. Microbiol. 2007; 53:1283–1290. [PubMed: 18059560]
4. Daugherty S, Low MG. Cloning, expression and mutagenesis of phosphatidylinositol-specific phospholipase C from *Staphylococcus aureus*: a potential staphylococcal virulence factor. Infect. Immun. 1993; 61:5078–5089. [PubMed: 8225585]
5. Lehto MT, Sharom FJ. PI-specific phospholipase C cleavage of a reconstituted GPI-anchored protein: modulation by the lipid bilayer. Biochemistry. 2002; 41:1398, 1408. [PubMed: 11802743]
6. Contreras FX, Sánchez-Magraner L, Alonso A, Goñi FM. Transbilayer (flip-flop) lipid motion and lipid scrambling in membranes. FEBS Lett. 2010; 584:1779–1786. [PubMed: 20043909]
7. Marques MB, Weller PF, Parsonnet J, Ransil B, Nicholson-Weller A. Phosphatidylinositol-specific phospholipase C, Phosphatidylinositol-specific phospholipase C, a possible virulence factor of *Staphylococcus aureus*. J. Clin. Microbiol. 1989; 27:2451–2454. [PubMed: 2808668]
8. Volwerk JJ, Shashidhar MS, Kuppe A, Griffith OH. Phosphatidylinositol-specific phospholipase C from from *Bacillus cereus* combines intrinsic phosphotransferase and cyclic phosphodiesterase activities: a ^{31}P NMR study. Biochemistry. 1990; 29:8056–8062. [PubMed: 2175645]

9. Zhou C, Qian X, Roberts MF. Allosteric activation of phosphatidylinositol-specific phospholipase C: specific phospholipid binding anchors the enzyme to the interface. Biochemistry. 1997; 36:10089–10097. [PubMed: 9254604]
10. Hondal RJ, Zhao Z, Kravchuk AV, Liao H, Riddle SR, Yue X, Bruzik KS, Tsai MD. Mechanism of phosphatidylinositol-specific phospholipase C: a unified view of the mechanism of catalysis. Biochemistry. 1998; 37:4568–4580. [PubMed: 9521777]
11. Dye EA, Kapral FA. Characterization of a bactericidal system in staphlococcal abscesses. Infect. Immun. 1980; 30:198–203. [PubMed: 6254879]
12. Heinz DW, Ryan M, Bullock TL, Griffith OH. Crystal structure of the phosphatidylinositol-specific phospholipase C from *Bacillus cereus* in complex with myoinositol. EMBO J. 1995; 14:3855–3863. [PubMed: 7664726]
13. Shi X, Shao C, Zhang X, Zambonelli C, Redfield AG, Head JF, Seaton BA, Roberts MF. Modulation of *Bacillus thuringiensis* phosphatidylinositol-specific phospholipase C activity by mutations in the putative dimerization interface. J. Biol. Chem. 2009; 284:15607–15618. [PubMed: 19369255]
14. Moser J, Gerstel B, Meyer JE, Chakraborty T, Wehland J, Heinz DW. Crystal structure of the phosphatidylinositol-specific phospholipase C from the human pathogen *Listeria monocytogenes*. J. Mol. Biol. 1997; 273:269–282. [PubMed: 9367761]
15. Feng J, Wehbi H, Roberts MF. Role of tryptophan residues in interfacial binding of phosphatidylinositol-specific phospholipase C. J. Biol. Chem. 2002; 277:19867–19875. [PubMed: 11912206]
16. Feng J, Bradley W, Roberts MF. Optimizing the interfacial binding and activity of a bacterial phosphatidylinositol-specific phospholipase C. J. Biol. Chem. 2003; 278:24651–24657. [PubMed: 12714598]
17. Guo S, Zhang X, Seaton BA, Roberts MF. Role of helix B residues in interfacial activation of a bacterial phosphatidylinositol-specific phospholipase C. Biochemistry. 2008; 47:4201–4210. [PubMed: 18345643]
18. Qian X, Zhou C, Roberts MF. Phosphatidylcholine activation of bacterial phosphatidylinositiol phospholipase C toward PI vesicles. Biochemistry. 1998; 37:6513–6522. [PubMed: 9572869]
19. Chen W, Goldfine H, Ananthanarayanan B, Cho W, Roberts MF. *Listeria monocytogenes* phosphatidylinositol-specific phospholipase C: Kinetic activation and homing in on different interfaces. Biochemistry. 2009; 48:3578–3592. [PubMed: 19281241]
20. Pu M, Orr A, Redfield AG, Roberts MF. Defining specific lipid binding sites for a peripheral membrane protein in situ using subtesla field-cycling NMR. J. Biol. Chem. 2010; 285:26916–26922. [PubMed: 20576615]
21. Crowley PB, Golovin A. Cation–π interactions in protein–protein interfaces. Proteins. 2005; 59:231–239. [PubMed: 15726638]
22. Rutledge LR, Churchill CDM, Wetmore SD. A preliminary investigation of the additivity of π-π or π+-π stacking and T-shaped interactions between natural or damaged DNA nucleobases and histidine. J. Phys. Chem. B. 2010; 114:3355–3367. [PubMed: 20151654]
23. Shi Z, Olson CA, Bell AJ, Kallenba NR. Stabilization of α-helix structure by polar side- chain interactions: complex salt bridges, cation–π interactions, and C–H ···O H-bonds. Biopolymers. 2001; 60:366–380. [PubMed: 12115147]
24. Singh JN, Min SS, Kim DY, Kim KS. Comprehensive energy analysis for various types of π-interaction. J. Chem. Theory Comput. 2009; 5:515–529.
25. Williams S, Bledsoe RK, Collins JL, Boggs S, Lambert MH, Miller AB, Moore J, McKee DD, Moore L, Nichols J, Parks D, Watson M, Wisely B, Willson TM. X-ray crystal structure of the liver X receptor β ligand binding domain: regulation by a histidine-tryptophan switch. J. Biol. Chem. 2003; 278:27138–27143. [PubMed: 12736258]
26. Hassan AQ, Koh JT. A functionally orthogonal ligand-receptor pair created by targeting the allosteric mechanism of the thyroid hormone receptor. J. Am. Chem. Soc. 2006; 128:8868–8874. [PubMed: 16819881]

27. Eckenroth BE, Steere AN, Chasteen ND, Everse SJ, Mason AB. How the binding of human transferrin primes the transferrin receptor potentiating iron release at endosomal pH. Proc. Natl. Acad. Sci. U.S.A. 2011; 108:13089–13094. [PubMed: 21788477]
28. Otwinowski Z, Minor W. Processing of X-ray diffraction data collected in oscillation mode. Methods Enzymol. 1997; 276:307–326.
29. Collaborative Computational Project, Number 4. The CCP4 Suite: programs for protein crystallography. Acta Crystallogr. D Biol. Crystallogr. 1994; 50:760–763. [PubMed: 15299374]
30. McCoy AJ, Grosse-Kunstleve RW, Adams PD, Winn MD, Storoni LC, Read RJ. Phaser crystallographic software. J. Appl. Cryst. 2007; 40:658–674. [PubMed: 19461840]
31. Brunger AT, Adams PD, Clore GM, DeLano WL, Gros P, Grosse-Kunstleve RW, Jiang JS, Kuszewski J, Nilges M, Pannu NS, Read RJ, Rice LM, Simonson T, Warren GL. Crystallography & NMR system: A new software suite for macromolecular structure determination. Acta Crystallogr. D Biol. Crystallogr. 1998; 54:905–921. [PubMed: 9757107]
32. Emsley P, Cowtan K. Coot: model-building tools for molecular graphics. Acta Crystallogr. D Biol. Crystallogr. 2004; 60:2126–2132. [PubMed: 15572765]
33. Adams PD, Afonine PV, Bunkóczi G, Chen VB, Davis IW, Echols N, Headd JJ, Hung LW, Kapral GJ, Grosse-Kunstleve RW, McCoy AJ, Moriarty NW, Oeffner R, Read RJ, Richardson DC, Richardson JS, Terwilliger TC, Zwart PH. PHENIX: a comprehensive Python-based system for macromolecular structure solution. Acta Crystallogr. D Biol. Crystallogr. 2010; 66:213–221. [PubMed: 20124702]
34. Schuettelkopf AW, van Aalten DMF. PRODRG - a tool for high-throughput crystallography of protein-ligand complexes. Acta Crystallogr. D Biol. Crystallogr. 2004; 60:1355–1363. [PubMed: 15272157]
35. Krissinel E, Henrick K. Secondary-structure matching (SSM), a new tool for fast protein structure alignment in three dimensions. Acta Crystallogr. D Biol. Crystallogr. 2004; 60:2256–2268. [PubMed: 15572779]
36. The PyMOL Molecular Graphics System, Version 1.3, Schrödinger, LLC.
37. Yang H, Guranovic V, Dutta S, Feng Z, Berman HM, Westbrook JD. Automated and accurate deposition of structures solved by X-ray diffraction to the Protein Data Bank. Acta Crystallogr. D Biol. Crystallogr. 2004; 60:1833–1839. [PubMed: 15388930]
38. Pu M, Roberts MF, Gershenson A. Fluorescence correlation spectroscopy of phosphatidylinositol-specific phospholipase C monitors the interplay of substrate and activator lipid binding. Biochemistry. 2009; 48:6835–6845. [PubMed: 19548649]
39. Honeyman, AL.; Friedman, H.; Bendinelli, M. Staphylococcus aureus Infection and Disease. New York: Kluwer Academic/Plenum Publishers; 2001.
40. Buriak C, Hammer CH, Robinson M-A, Whitney AR, McGavin MJ, Kreiswirth BN, DeLeo FR. Global analysis of community-associated methicillin-resistant *Staphylococcus aureus* exoproteins reveals molecules produced in vitro and during infection. Cell. Microbiol. 2007; 9:1172–1190. [PubMed: 17217429]

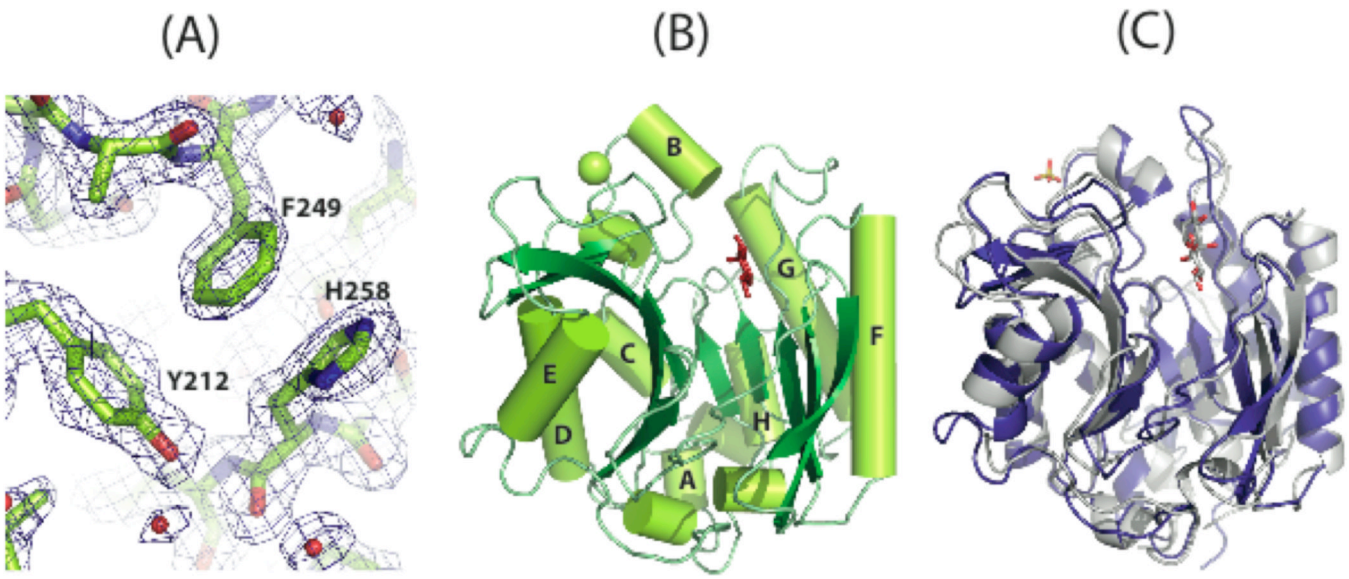

Figure 1.

(A) Representative electron density of the rim loop of the acidic model, view of the π-cation interaction residues. Electron density of part of the rim loop in the acid pH atructure, shown in dark blue and contoured at 1σ, is shown with the model superimposed. (B) Overall structure of the acidic form of *S. aureus* PI-PLC with the helix notation used in the structure of *L. monocytogenes* PI-PLC (pdb 2PLC) (14). Myo-inositol in red is shown bound to the active site; the chloride ion is shown as a green sphere occupying the cationic rim pocket. (C) Comparison of basic form of *S. aureus* PI-PLC (blue) and *B. cereus* PI-PLC (silver), pdb 1GYM. The glucosamine-α1,6-*myo*-inositol ligand seen in 1GYM is shown in stick representation; the inositol ring marks the active sites of the enzymes.

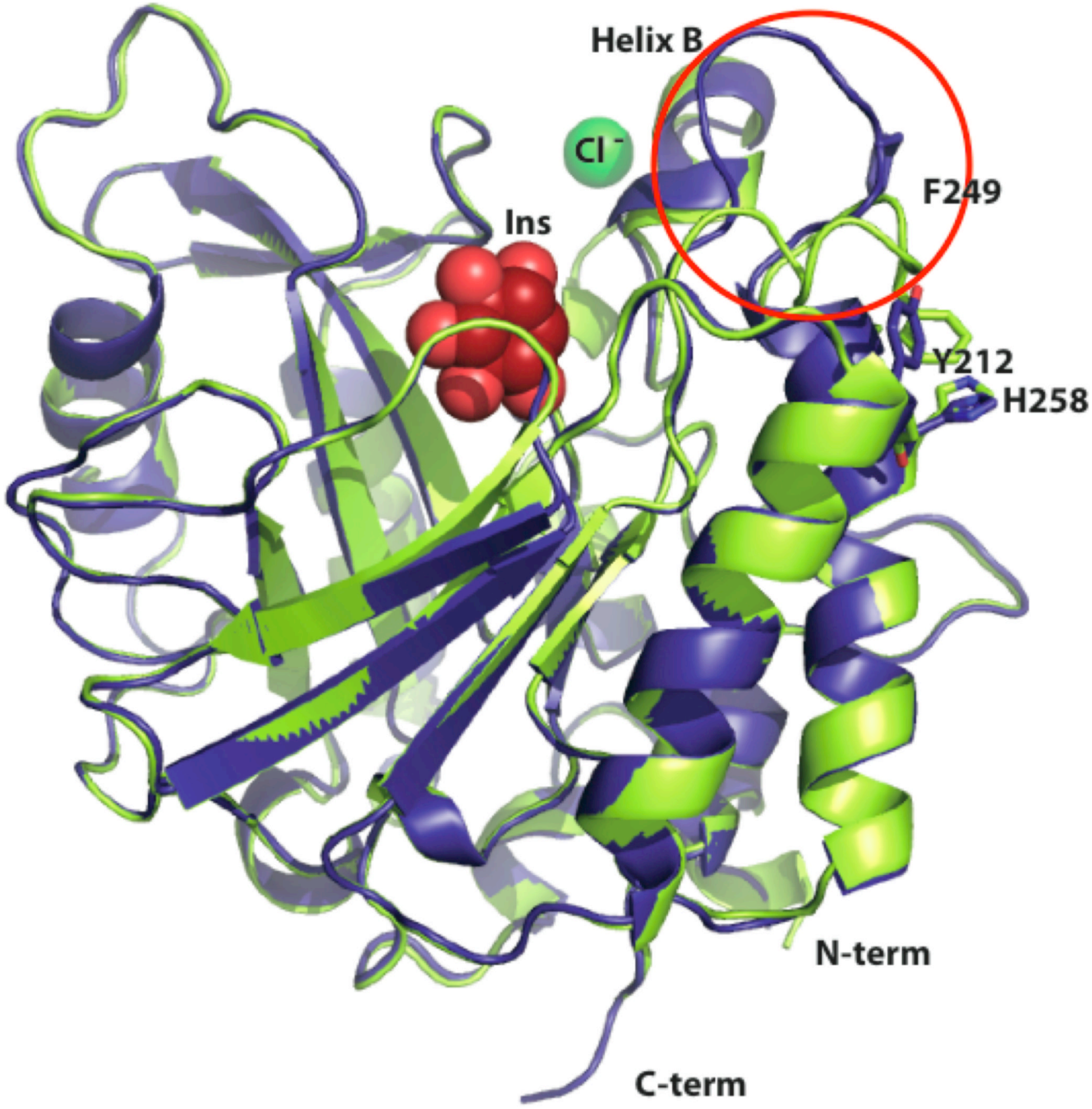

Figure 2.
Overlay of the acidic pH (green) and basic pH (blue) structures of *S. aureus* PI-PLC. The red circle highlights the mobile rim loop and the large conformational change in it with pH. Key residues forming the π-cation interaction are labeled. Myo-inositol is depicted in red spacefilling representation and the chloride ion as a green sphere. The C and N terminals, and helix B are labeled. A grey bar represents the membrane interface.

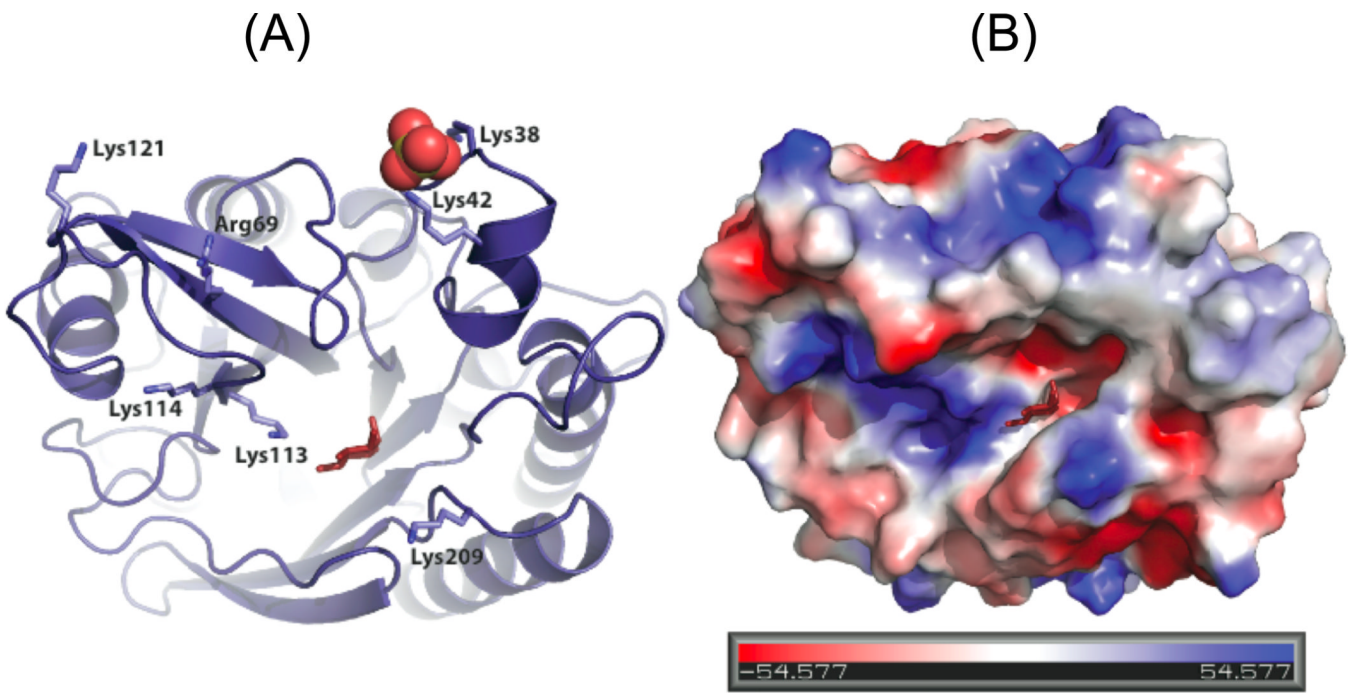

Figure 3.

(A) Cationic residues around the rim of the βα barrel of *S. aureus* PI-PLC at pH 7.5, as seen from the membrane interface. These residues create an electropositive region, contributing to electrostatic binding of the protein to the membrane. Myo-inositol shown in red stick orientation indicates the active site, and the sulfate ion is shown as red spheres. (B) Electrostatic map of the unliganded protein as seen from the same orientation. Regions of positive charge around the barrel rim can be seen in blue.

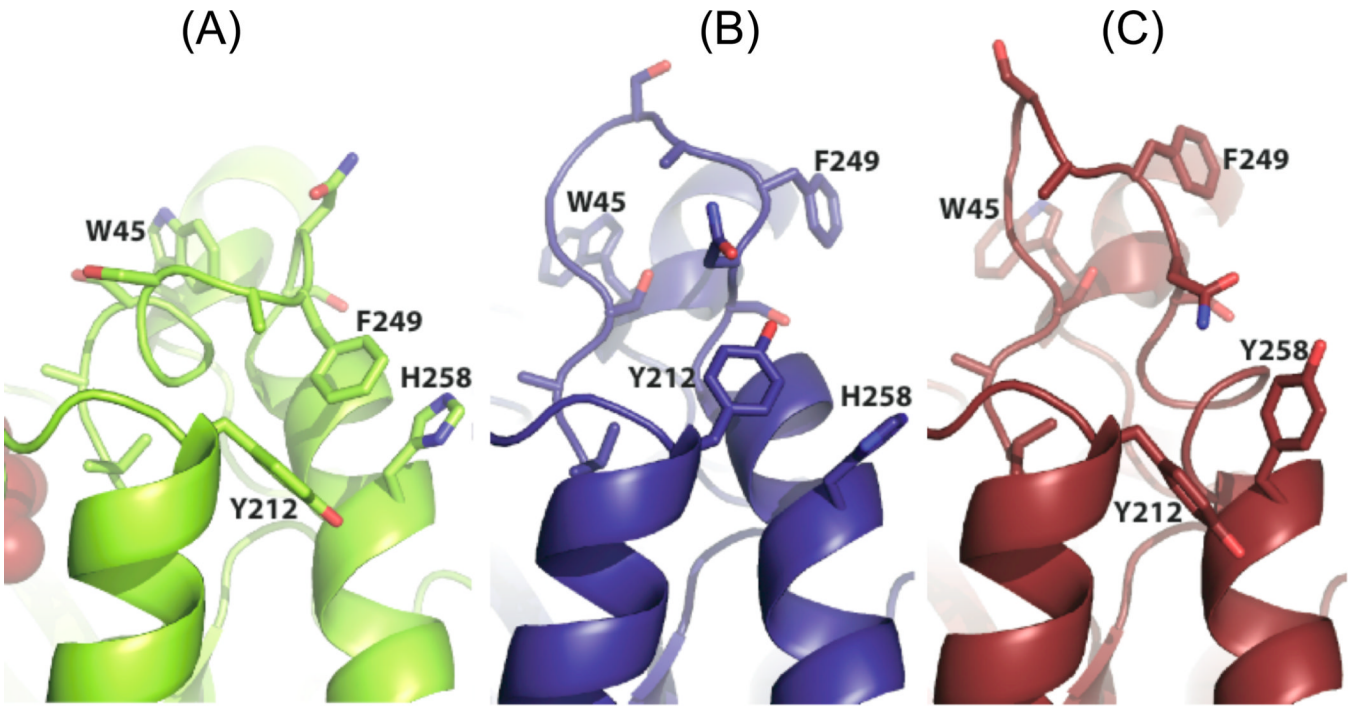

Figure 4.

A close-up of the *S. aureus* PI-PLC mobile rim loop conformation near helices F and G in the wild type enzyme at (A) pH 4.6 and (B) pH 7.5, compared to the same region in the H258Y structure at pH 4.6 (C). The proposed Phe249 / His258 π-cation interaction and relevant side-chains are indicated in each panel.

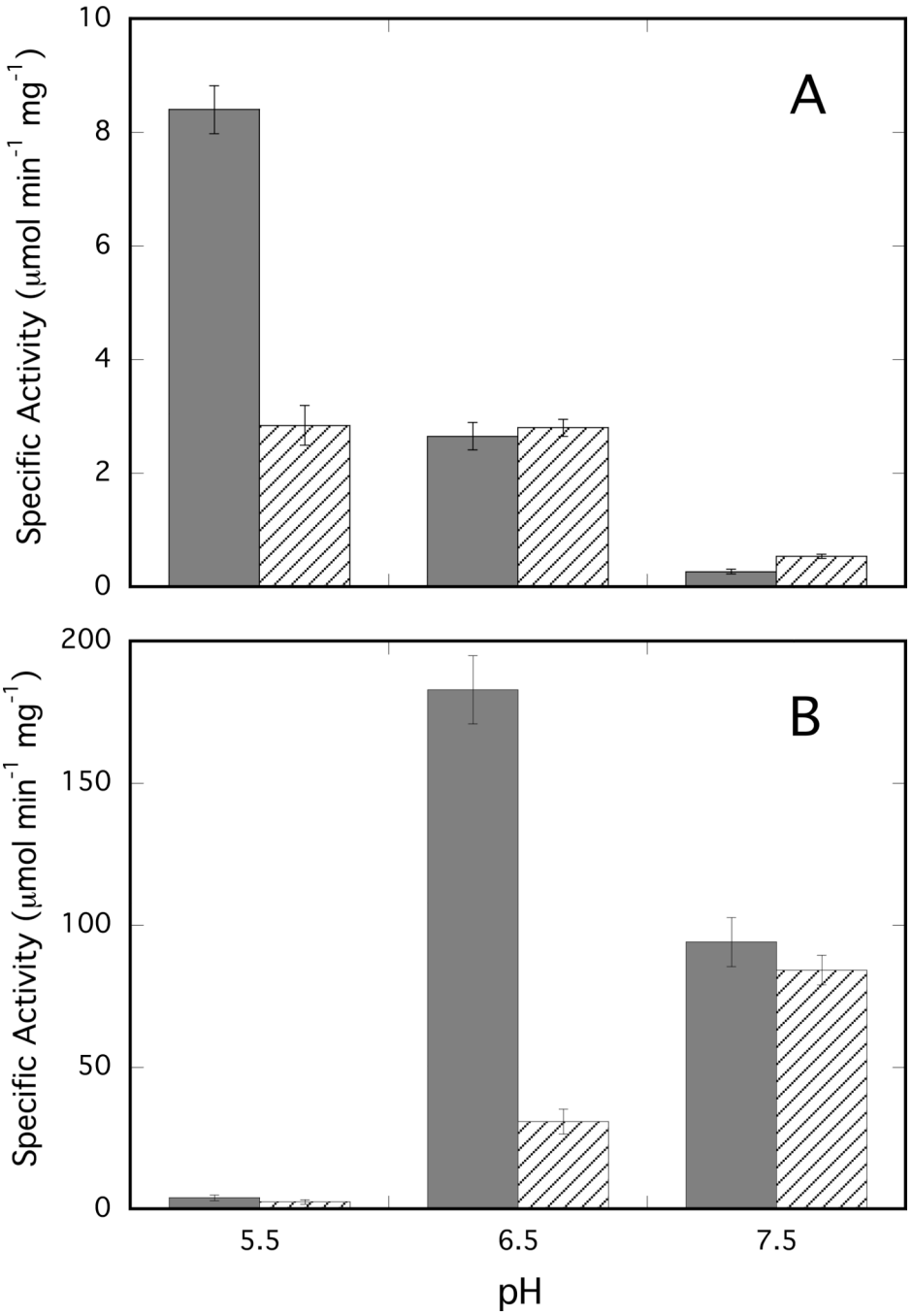

Figure 5.

The pH dependence of the specific activity of *S. aureus* recombinant PI-PLC and the H258Y mutant towards (A) 4 mM PI and (B) PI/PC (4 mM:1 mM) small unilamellar vesicles in 50 mM MES/HEPES, 1 mM EDTA with 0.1 mg/ml BSA adjusted to the indicated pH. Wild type enzyme activities are the gray bars with the H258Y mutant shown as the hatched bars.

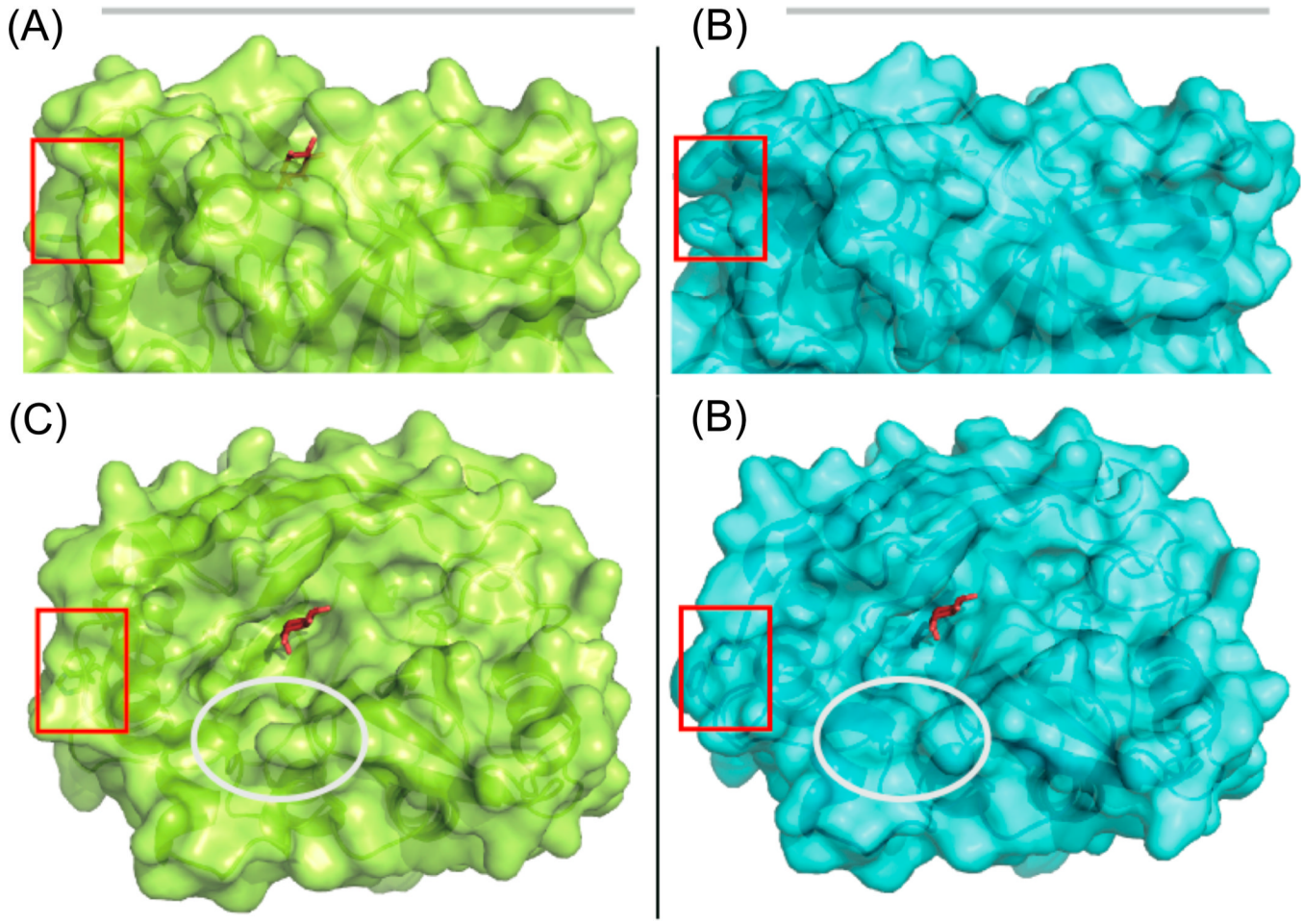

Figure 6.
Space filling models depicting the active site wall channel for native structures. Structures at pH 4.6 are shown (A) juxtaposed to the membrane, which is represented by a grey bar, and looking down into the αβ barrel, as seen from the membrane interface (C), with the active site channel location marked with a grey oval. The same set of orientations are shown for the pH 7.5 structure, with the view (B) facing the membane and (D) looking down from the membrane interface. Myo-inositol, red stick representation, is visible in both views from the membrane, but not in the basic structure seen form the side. The location of the key π-cation residues is shown as a red box.

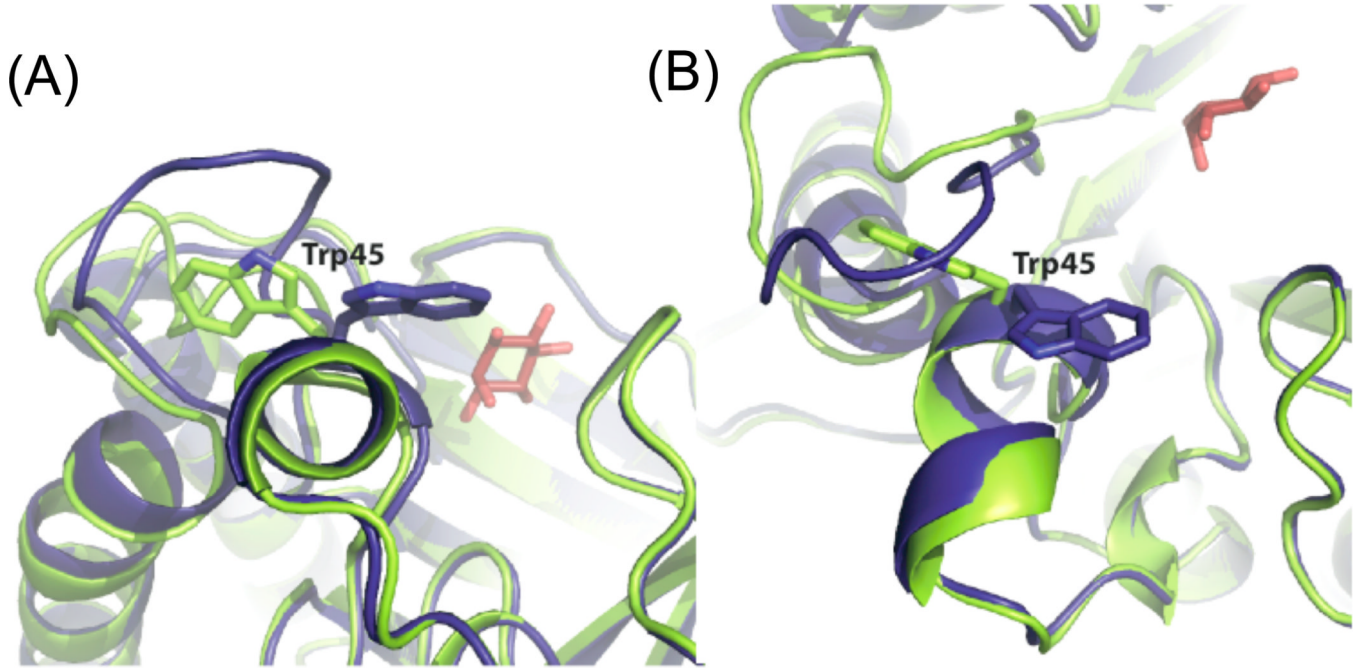

Figure 7.
Trp45 gate shown as a cartoon with Trp45 sidechain shown as sticks. Both top down (A) and sideways (B) views are shown. The position of the mobile loop in the acidic structure (green) allows the Trp45 side chain to open, while the possition of the mobile loop in the basic strucutre (blue) forces the Trp45 side chain into the closed positon, sealing off the active site. Insoitol is seen in red in the background.

Table 1

Full refinement and model statstics.

		Acidic	Basic	H258Y
PDB ID Code		**3V16**	**3V18**	**3V1H**
Diffraction Data				
	Resolution range (Å)	39.9-2.3	48.0-2.34	34.9-1.9
	No. of reflections	17112	12534	23280
	No. of reflections in free set	923	648	1246
	Space group	$P2_12_12_1$	$P2_12_12_1$	$P2_12_12_1$
	Unit cell			
	a(Å)	104.16	85.35	87.95
	b(Å)	43.61	58	57.22
	c(Å)	62.22	61.72	61.14
	Completeness	97.1	98.4	97.7
	R_{merge}	0.045	0.119	0.093
Refinement	R_{cryst} *a*	0.1555	0.1820	0.1867
	R_{free} *b*	0.2131	0.2566	0.2374
	No. of residues	303	304	306
	No. of non-hydrogen protein atoms	2445	2431	2476
	No. of non-hydrogen inositol atoms	12	0	12
	No. of H_2O molecules	225	156	265
	No. of ions	1	1	2
	r.m.s.d. bonds (Å)	0.022	0.018	0.023
	r.m.s.d angles (°)	1.7	1.7	1.8
	Ramachandran plot %			
	Most favored	89.0	89.4	90.9
	Additionally allowed	11.0	13.6	9.1
	Generously allowed	0	0.4	0
	Disallowed	0	0	0
	Average B-factor ($Å^2$)	28.5	41.0	27.1

a $R_{cryst} = \{\Sigma (||F_O| - |F_C||) / |F_O|\}$, where $|F_O|$ and $|F_C|$ are the observed and calclated structure factor amplitudes, respectively.

b Brunger (1992)